Monthly Notices
of the
ROYAL ASTRONOMICAL SOCIETY

MNRAS **470,** 401–415 (2017)
Advance Access publication 2017 May 18

doi:10.1093/mnras/stx1197

The evolution of CNO isotopes: a new window on cosmic star formation history and the stellar IMF in the age of ALMA

D. Romano,[1]★ F. Matteucci,[2,3,4] Z.-Y. Zhang,[5,6] P. P. Papadopoulos[6,7,8] and R. J. Ivison[5,6]

[1] *INAF, Osservatorio Astronomico di Bologna, Via Gobetti 93/3, I-40129 Bologna, Italy*
[2] *Dipartimento di Fisica, Sezione di Astronomia, Università di Trieste, Via Tiepolo 11, I-34131 Trieste, Italy*
[3] *INAF, Osservatorio Astronomico di Trieste, Via Tiepolo 11, I-34131 Trieste, Italy*
[4] *INFN, Sezione di Trieste, Via Valerio 2, I-34127 Trieste, Italy*
[5] *Institute for Astronomy, University of Edinburgh, Royal Observatory, Blackford Hill, Edinburgh EH9 3HJ, UK*
[6] *European Southern Observatory, Karl-Schwarzschild-Str. 2, D-85748 Garching bei München, Germany*
[7] *School of Physics and Astronomy, Cardiff University, Queen's Buildings, The Parade, Cardiff CF24 3AA, UK*
[8] *Section of Astrophysics, Astronomy and Mechanics, Department of Physics, Aristotle University of Thessaloniki, Thessaloniki 54124, Greece*

Accepted 2017 May 12. Received 2017 March 15; in original form 2016 December 23

ABSTRACT

We use state-of-the-art chemical models to track the cosmic evolution of the CNO isotopes in the interstellar medium of galaxies, yielding powerful constraints on their stellar initial mass function (IMF). We re-assess the relative roles of massive stars, asymptotic giant branch (AGB) stars and novae in the production of rare isotopes such as ^{13}C, ^{15}N, ^{17}O and ^{18}O, along with ^{12}C, ^{14}N and ^{16}O. The CNO isotope yields of super-AGB stars, novae and fast-rotating massive stars are included. Having reproduced the available isotope enrichment data in the solar neighbourhood, and across the Galaxy, and having assessed the sensitivity of our models to the remaining uncertainties, e.g. nova yields and star formation history, we show that we can meaningfully constrain the stellar IMF in galaxies using C, O and N isotope abundance ratios. In starburst galaxies, where data for multiple isotopologue lines are available, we find compelling new evidence for a top-heavy stellar IMF, with profound implications for their star formation rates and efficiencies, perhaps also their stellar masses. Neither chemical fractionation nor selective photodissociation can significantly perturb globally averaged isotopologue abundance ratios away from the corresponding isotope ones, as both these processes will typically affect only small mass fractions of molecular clouds in galaxies. Thus, the Atacama Large Millimeter Array now stands ready to probe the stellar IMF, and even the ages of specific starburst events in star-forming galaxies across cosmic time unaffected by the dust obscuration effects that plague optical/near-infrared studies.

Key words: nuclear reactions, nucleosynthesis, abundances – stars: luminosity function, mass function – Galaxy: abundances – Galaxy: evolution – galaxies: star formation.

1 INTRODUCTION

Measurements of isotope abundances and abundance ratios allow us to perform key tests of mixing mechanisms inside stars, and provide powerful diagnostics of chemical enrichment in galaxies across cosmic time. Some carry valuable information about the state of the early Universe, which can be used to probe fundamental physics. Determinations of the ^{6}Li/^{7}Li ratios in metal-poor stars (Cayrel et al. 2007; García Pérez et al. 2009; Lind et al. 2013), for instance, constrain big bang nucleosynthesis theories (Cyburt et al. 2016) and the degree of ^{7}Li depletion possible in Galactic halo stars (Spite & Spite 2010). The CNO isotope ratios measured in presolar grains (Clayton & Nittler 2004; Zinner 2014) and in the atmospheres of evolved stars (Gratton et al. 2000; Smiljanic et al. 2009, and references therein) can be compared to expectations from stellar evolution and nucleosynthesis models to shed light on the nature of non-standard mixing processes acting on the giant branches (see Charbonnel 1994; Wasserburg, Boothroyd & Sackmann 1995; Charbonnel & Zahn 2007; Palmerini et al. 2009, among others). Peculiar isotopic features in C-rich grains can be explained by considering the effects of hydrogen ingestion into the helium shell of core-collapse supernovae before the shock hits the outer layers (Pignatari et al. 2015). Beginning with Boesgaard (1968), magnesium isotope

★ E-mail: donatella.romano@oabo.inaf.it

abundances have been measured in stars in order to provide insights into the production sites of the two minor, neutron-rich isotopes, ^{25}Mg and ^{26}Mg. Last but not least, measurements of barium (Gallagher et al. 2015, and references therein), europium, samarium and neodymium isotope ratios in stars (Roederer et al. 2008) allow us to establish whether the dominant formation process is slow or rapid neutron capture by heavy seed nuclei, thus contributing significantly to our understanding of how neutron-capture elements are created in galaxies.

In principle, large samples of stars with precise chemical abundances over the full range of plausible metallicities should provide a complete fossil record of the history of chemical enrichment for their host galaxies (provided the data are corrected for stellar evolutionary effects when needed; see Placco et al. 2014). Alongside accurate determinations of stellar ages, distances and kinematics, abundance data can meaningfully constrain models of galaxy formation and evolution (Freeman & Bland-Hawthorn 2002; Ivezić, Beers & Jurić 2012). However, when it comes to the determination of isotopic abundance ratios in stars, very high resolution, high signal-to-noise spectroscopic data are invariably needed, which severely limits current observational studies. It is then useful to turn to measures of the gas-phase isotopic abundances in interstellar clouds, which enables us to look significantly further afield. On the other hand, each observation provides merely a snapshot in time, and information about the temporal sequence of events that led to the observed configuration is thus missing. Based on these diagnostics, however, crucial information on the present-day gradients of ^{12}C/^{13}C, ^{14}N/^{15}N, ^{16}O/^{18}O and ^{18}O/^{17}O across the Milky Way disc can be obtained (Wilson & Rood 1994).

Indeed, in the era of the Atacama Large Millimeter Array (ALMA), it has become possible to peer back to the epoch when gas-rich galaxies dominated the Universe, at $z > 1$, which should lead to a better understanding of the evolutionary links between these galaxies and their descendants. Exploiting isotopologue line intensity ratios as probes of the corresponding elemental isotope ratios will open a new window on to the isotope enrichment history of the Universe across cosmic epoch. Such observations were already plentiful in the local Universe, even before ALMA (e.g. Sage, Mauersberger & Henkel 1991; Casoli, Dupraz & Combes 1992; Henkel & Mauersberger 1993; Aalto et al. 1995; Papadopoulos, Seaquist & Scoville 1996; Paglione et al. 2001; Greve et al. 2009), and now extend out to $z \sim 3$ (Henkel et al. 2010; Spilker et al. 2014; Zhang et al., in preparation). Even more importantly, isotopologue line ratios are the *only* probe of isotope ratios that are unaffected by dust extinction, as isotopologue lines (e.g. ^{12}CO, ^{13}CO, C^{18}O, H^{13}CN, HC^{15}N rotational transitions) are found in the millimetre/submillimetre (submm) regime. Besides the obvious advantage of a method insensitive to dust extinction, it is in the highly dust-enshrouded star-forming environments of compact starbursts (e.g. Ikarashi et al. 2015; Simpson et al. 2017) where *very different average initial conditions of star formation* (Papadopoulos 2010) can lead to a different stellar initial mass function (IMF; see Papadopoulos et al. 2011). Yet it is exactly in these dust-obscured galaxies where the stellar IMF is inaccessible via standard methods (e.g. star counts) and where the different isotope enrichment of the interstellar medium (ISM) would provide the best evidence for a different stellar IMF. In short, in the dust-obscured environments of star-forming galaxies, isotope abundance ratios provide the next best constraint on the prevailing stellar IMF, other than starlight itself. This prevailing IMF is important to our understanding of galaxy evolution since it is a key ingredient of the recipes used to determine the instantaneous star formation rate, for example, where extrapolations are made from the number of massive stars to the total mass of stars. The evolution of galaxies is often explored in the observational framework of the so-called main sequence (e.g. Elbaz et al. 2011), plotted usually as star formation rate versus stellar mass. Where both measurements are sensitive to the IMF, the implications may be profound.

In past years, many theoretical efforts (including Audouze, Lequeux & Vigroux 1975; Dearborn, Tinsley & Schramm 1978; Tosi 1982; Matteucci & D'Antona 1991; Wilson & Matteucci 1992; Timmes, Woosley & Weaver 1995; Prantzos, Aubert & Audouze 1996; Fenner et al. 2003; Romano & Matteucci 2003; Chiappini et al. 2008; Hughes et al. 2008; Kobayashi, Karakas & Umeda 2011) have been devoted to the evolution of isotope ratios in the Galaxy. Hughes et al. (2008) also discuss observations of carbon and sulphur isotopes in a spiral galaxy and a damped Lyα system (DLA) at $z \sim 1$. Although there is no doubt that progress has been made, some questions remain unanswered. For example, we know that ^{12}C is produced as a primary element in stars (i.e. starting from the original H and He; Burbidge et al. 1957) and that the relative contributions from low- and intermediate-mass stars and from massive stars change with time and position within the Galaxy (e.g. Akerman et al. 2004); the actual proportions are still debated, however.

Regarding ^{14}N, it has been acknowledged for a long time that significant primary nitrogen production is needed to explain observations of low-metallicity systems (e.g. Edmunds & Pagel 1978; Matteucci 1986). The physical process responsible for this production remained elusive for decades, until very low metallicity, fast-rotating massive star models proved able to convert part of the freshly made ^{12}C into primary ^{14}N (and ^{13}C), quite efficiently, because of rotation-induced mixing between the convective hydrogen shell and the helium core (Meynet & Maeder 2002a; Chiappini et al. 2008). However, chemical evolution models that adopt ^{14}N yields from fast-rotating stellar models still predict a much lower nitrogen abundance in the ISM than observed in the metallicity range $-2.5 <$ [Fe/H] < -1.5 (Chiappini et al. 2006; Romano et al. 2010). In intermediate-mass stars climbing the asymptotic giant branch (AGB), proton-capture nucleosynthesis leads to primary ^{14}N (and ^{13}C) production if the base of the convective envelope becomes hot enough (a process referred to as hot bottom burning; see Iben 1975). Moreover, a large fraction of ^{14}N is synthesized as a secondary element, at the expense of ^{12}C, through the CN cycle in stars of all masses and – at a much slower rate – at the expense of ^{16}O in the ON cycle. Adding these contributions, however, does not help to solve the aforementioned problem.

Another outstanding issue is that of ^{15}N evolution. Novae have been identified as ^{15}N polluters on a Galactic scale (Dearborn et al. 1978; Matteucci & D'Antona 1991; Romano & Matteucci 2003), but observations of low ^{14}N/^{15}N at high redshift (Muller et al. 2006) suggest an additional production channel, possibly hydrogen ingestion in the helium shell of massive stars (Pignatari et al. 2015).

The synthesis of ^{16}O in stars, on the other hand, is well understood, both qualitatively and quantitatively, and chemical evolution models can fit the relevant data, regardless of the specific set of yields adopted (see fig. 8 of Romano et al. 2010). The less abundant, neutron-rich oxygen isotopes, ^{17}O and ^{18}O, are made as secondary elements by the CNO cycle during hydrogen burning and by α-captures on ^{14}N during helium burning, respectively. While intermediate-mass stars, massive stars and novae all contribute significantly to ^{17}O production, the situation for ^{18}O is less clear; it seems, in fact, that intermediate-mass stars destroy ^{18}O rather than produce it.

In this work, we focus on the evolution of the CNO isotopes in the ISM of galaxies – those associated with the most abundant molecule after H_2, namely carbon monoxide (CO). First, we re-assess the relative roles of massive stars, AGB stars and novae in the production of the rare isotopes ^{13}C, ^{15}N, ^{17}O and ^{18}O on a Galactic scale, in the light of newly published stellar yields and more recent isotopic abundance determinations in the Milky Way. Secondly, we discuss how new measurements of ^{12}C/^{13}C and ^{16}O/^{18}O ratios in starburst galaxies can constrain their stellar IMF. We stress that these constraints on the stellar IMF are ultimately set by the stellar physics underlying the chemical evolution model, and as such are extremely powerful, regardless of remaining uncertainties. In this work, we examine these uncertainties, focusing on the assumed stellar yields, star formation histories and the astrochemical effects on molecules, such as fractionation and selective photodissociation. These two effects, if widespread, could in principle prevent us from directly deducing isotope abundance ratios from the corresponding isotopologues. In the age of ALMA, numerous isotopologue line ratios can now be measured for the molecular gas of dust-obscured galaxies, where there is no hope of measuring the stellar IMF directly via star counts or integrated starlight, leaving these ratios as the next best thing for constraining the IMF (Papadopoulos et al. 2014).

The paper is organized as follows: in Section 2, we review the available data. In Section 3, we briefly describe the chemical evolution models. In Section 4, we present the model results and compare them to data for both the Milky Way (Section 4.1) and other galaxies (Section 4.2), with special emphasis on intense starburst galaxies. We discuss our findings and conclusions in Section 5.

2 OBSERVATIONAL DATA

2.1 Milky Way galaxy

The ^{12}C/^{13}C ratio does not display significant variability within the Solar system; we adopt the value inferred from CO infrared (IR) lines in the solar spectrum using 3D convection models (91.4±1.3; Ayres et al. 2013) as indicative of the ISM composition in the solar vicinity 4.5 Gyr ago. Observations of CO, H_2CO (taken from the compilation of Wilson & Rood 1994), CO_2 (from Boogert et al. 2000) and CN (Savage et al. 2002; Milam et al. 2005) and their ^{13}C-bearing isotopologues are used to trace the behaviour of the ^{12}C/^{13}C ratio across the disc of the Galaxy at the present time. The gradients derived from CO and CN agree closely, which, together with the lack of correlation of the ratios with gas kinetic temperature, $T_{\rm kin}$, suggests that the effects of chemical fractionation and isotope-selective photodissociation are negligible (Milam et al. 2005). Indeed, there are simple reasons why these two astrochemical effects cannot significantly perturb isotopologue abundance ratios from the corresponding isotopic ratios for the bulk of the molecular gas reservoir in galaxies, which we briefly outline in Section 2.3.

The ^{12}C/^{13}C ratios derived from both H_2CO and CO_2 tend to be higher than those derived from other tracers (Boogert et al. 2000). The carbon isotope ratio varies significantly in the local ISM; we take the average value of ^{12}C/^{13}C = 68 ± 15 suggested by Milam et al. (2005) as typical of the local ratio. It is worth noting that because of the significant heterogeneity in interstellar carbon isotope ratios, it is unclear whether the solar value is truly representative of the average local ^{12}C/^{13}C ratio 4.5 Gyr ago. On top of that, the Sun might have migrated to its current position from a birthplace closer to the Galactic Centre (Wielen, Fuchs & Dettbarn 1996) and its composition could thus reflect chemical enrichment occurring on faster time-scales. Measurements of ^{12}C/^{13}C ratios in statistically significant samples of nearby dwarf stars would usefully constrain the models, but they are challenging. In brighter, giant stars, on the other hand, mixing may have altered the original abundances. In this paper, we use ^{12}C/^{13}C data from Spite et al. (2006) for a sample of 'unmixed' halo giants, i.e. stars lying mostly on the low red giant branch where the original CNO abundances were likely unaltered by mixing processes.

The nitrogen isotope ratio presents extreme variations among different Solar system objects (e.g. Füri & Marty 2015); we adopt as a proxy for the protosolar nebula the estimate for the bulk Sun from Marty et al. (2011), namely ^{14}N/^{15}N = 441 ± 6. Considerations discussed in the previous paragraph about the representativeness of the solar ^{12}C/^{13}C ratio also apply to the ^{14}N/^{15}N ratio. Accurate measurements of the ^{14}N/^{15}N ratios towards warm molecular clouds spanning a range of Galactocentric distances have been obtained by Adande & Ziurys (2012) from millimetre-wave observations of rotational lines of CN and HNC and their isotopologues. Direct (from CN, correcting for opacities when needed) and indirect (from HNC, using the ^{12}C/^{13}C ratios previously established by Milam et al. 2005, for each source) determinations yield the same gradient, within the uncertainties. The ^{14}N/^{15}N ratios derived by Adande & Ziurys (2012), however, are systematically lower than those obtained by Dahmen, Wilson & Matteucci (1995) from H^{13}CN/HC^{15}N data, likely because of the use of ^{12}C/^{13}C ratios from H_2CO in Dahmen et al. (1995). Indeed, scaling the HCN data of Dahmen et al. (1995) with ^{12}C/^{13}C ratios from CN yields HCN values that agree with those from the other indicators, within the uncertainties (see fig. 3 of Adande & Ziurys 2012). It is worth noting that, while Romano & Matteucci (2003) had to offset their model predictions to match Dahmen et al. (1995) data, the new estimates of the ^{14}N/^{15}N ratio across the Galaxy by Adande & Ziurys (2012) make such a correction unnecessary. The mean local ISM value suggested by Adande & Ziurys (2012), ^{14}N/^{15}N = 290 ± 40, agrees with that measured in nearby diffuse clouds from CN absorption lines in the optical (274±18; Ritchey, Federman & Lambert 2015).

We adopt the solar photospheric ratios ^{16}O/^{18}O = 511 ± 10 and ^{18}O/^{17}O = 5.36 ± 0.34 from Ayres et al. (2013) as indicative of the local ISM composition 4.5 Gyr ago. A radial ^{18}O/^{17}O gradient is suggested by Wouterloot et al. (2008), who combine observations of different CO transitions in Galactic sources covering the Galactocentric distance range $0 < R_{\rm GC}/{\rm kpc} < 17$. Their finding is further supported by recent independent analysis and observations by Li et al. (2016). Ratios of ^{16}O to ^{18}O across the disc are taken from the compilation of Wilson & Rood (1994), from OH data of Polehampton, Baluteau & Swinyard (2005), and derived by combining the CO data from Wouterloot et al. (2008) with the ^{12}C/^{13}C gradient from Milam et al. (2005) following Young et al. (2011).

2.2 Other galaxies

CNO isotopic abundances can be precisely measured on the Earth and in the Sun. However, they are more difficult to obtain in the Galactic ISM and – even more so – in the extragalactic ISM, due to the limits of past observational capabilities and the high optical depths of the molecular lines of the most abundant isotopologues. Because of past sensitivity limitations, measurements of the extragalactic isotopic CO transitions have been limited to local gas-rich and metal-enriched galaxies (e.g. Paglione et al. 2001; Costagliola et al. 2011; Tan et al. 2011; Davis 2014). With the help of

gravitational lensing, which can greatly amplify the flux densities, isotopic lines at $z > 2$ have now been measured in a few cases (Muller et al. 2006; Henkel et al. 2010; Danielson et al. 2013).

Isotopic abundances are difficult to derive from the measured molecular lines, especially for the ^{12}C-bearing species, which are the most abundant and thus their transitions have the highest opacities. Observed line ratios do not translate directly to the abundance ratios – one needs to correct for the unknown optical depths. As a result, the ^{12}C/^{13}C and ^{16}O/^{18}O abundance ratios from the line ratios are often significantly underestimated. The most straightforward method to derive the optical depths and obtain the isotopic abundance ratios uses the line ratios between the optically thin double isotopologue (e.g. ^{13}C^{18}O) and a single isotopic molecular line (e.g. C^{18}O) of the same quantum transition. However, should the isotopologue line (e.g. C^{18}O) not be completely optically thin, would mean an underestimate of the derived ^{12}C/^{13}C abundance ratio. Moreover, the emission lines from the double isotopologues are so weak that it has only been possible to detect them in a few bright targets, even with the most sensitive radio telescopes (e.g. M82, NGC 253; Martín et al. 2010). ALMA will improve this situation considerably, but a large survey of nearby normal galaxies, or high-redshift star-forming galaxies, will remain difficult, unless lensed objects are used in the latter case.

A second method derives the abundance ratios using the absorption features of molecular isotopologues against strong radio continuum sources. This is perhaps the most accurate method to derive the column densities from the measured equivalent widths, as measured directly from the isotopologues. This method is also insensitive to distance and angular resolution. Its main drawback, however, is that a very strong background source is needed. Only the combination of galactic ISM in the line of sight to the brightest radio-loud quasars, or very strong continuum emission from the target itself, is adequate for such studies. This method has been used to measure the diffuse ISM in our Milky Way galaxy (e.g. Lucas & Liszt 1996, 1998), local galaxies (e.g. González-Alfonso et al. 2012) and a few distant galaxies (e.g. Wiklind & Combes 1995, 1996; Muller et al. 2014). Targets lending themselves to such studies are thin on the ground because of the rare configuration requirements. Optical observations of DLA absorbers also present the ability to probe isotopologue ratios in high-z objects (Levshakov et al. 2006; Noterdaeme et al. 2017).

A third method requires two steps, deriving the optical depths and the abundance ratios separately using the N-bearing molecular line. Most often, ^{13}CN, ^{12}CN $N = 1$–0 and its hyperfine structure lines are observed, and the optical depth of ^{12}CN is derived. Then the opacity-corrected ^{12}CN is compared with the emission of ^{13}CN, which is assumed to be optically thin. Their ratio yields the ^{12}C/^{13}C abundance ratio, which can be further converted to the ^{16}O/^{18}O ratio using observations of ^{13}CO and C^{18}O (e.g. Savage et al. 2002; Milam et al. 2005). However, this method relies on measurements of the CN molecule, which requires high-density conditions ($n_{\rm crit}^{\rm CN\,1-0} \sim 10^{4-5}$ cm^{-3}; Shirley 2015) like those found in the dense cores of star-forming regions, where optical depths are also high. Furthermore, the assumption of an optically thin ^{13}CO may not always hold, as with the first method.

A fourth method models the average gas physical conditions using multiple rotational transitions of the isotopologues and radiative transfer models based on the large velocity gradient (LVG) approximation (Goldreich & Kwan 1974; Scoville & Solomon 1974) or the mean-escape probability approximation (Osterbrock 1989; Curran et al. 2001). This allows an estimate of the optical depths of both the major and minor isotopologues, which allows the appropriate correction of the observed line ratios to get the abundance ratios. It is much easier to obtain multiple transitions of CO isotopologues rather than for other even rarer molecules. However, because of the degeneracy of the collisional coefficient between density and temperature, $C \propto n_{\rm H_2} T_{\rm kin}^{1/2}$, the degeneracy between molecular abundances and other gas properties (e.g. average dV/dR) that set a given line optical depth, and the assumption of uniformly distributed physical conditions in studied regions, the uncertainty of the deduced abundance ratio can be considerable. Moreover, in the case of the CO/^{13}CO (or CO/C^{18}O) line ratio, the stronger radiative trapping expected for the much more abundant CO than for ^{13}CO can also play some role in boosting their values in some galaxies in addition to enhanced global CO/^{13}CO abundances in their ISM (e.g. Aalto et al. 1995).

In Table 1, we list the abundance ratios published in the literature. There are many detections of a single transition of ^{13}CO in galaxies, both in their centres and in the off-nuclear arm/disc regions (e.g. Paglione et al. 2001; Tan et al. 2011; Davis 2014). In this study, we adopt only the abundance ratios; we neglect the line ratios that, in principle, could be used to set the lower limits.

2.3 From isotopologue to isotope abundance ratios: the road is now clear

The first detections of isotopologue ^{13}CO and C^{18}O line emission in the Galaxy (Penzias, Jefferts & Wilson 1971) were soon followed by numerous detections of other, more distant galaxies (Encrenaz et al. 1979; Rickard & Blitz 1985; Young & Sanders 1986; Sage & Isbell 1991; Wall et al. 1993; Aalto et al. 1995; Papadopoulos et al. 1996; Papadopoulos & Seaquist 1998; Paglione et al. 2001). This facilitated the use of isotopologue abundance ratios as direct measures of isotope abundance ratios in the ISM of other galaxies (see Langer & Penzias 1993, for Galactic studies of the ^{13}CO, ^{12}CO isotopologues). It was this new observational capability, and the discovery that ^{12}CO/^{13}CO *intensity* ratios are typically much larger in extreme merger/starburst galaxies than in ordinary star-forming spirals (Casoli et al. 1992; Henkel & Mauersberger 1993; Henkel et al. 1993; Aalto et al. 1995; Papadopoulos & Seaquist 1998), that triggered investigations into whether or not isotopologue abundance ratios translate directly to isotopic ratios (e.g. [^{12}CO/^{13}CO] = [^{12}C/^{13}C]).

Two astrochemical effects stand in the way of obtaining an isotope abundance ratio from the corresponding isotopologue abundance ratio, namely (1) selective photodissociation of the rarer isotope (Casoli et al. 1992) and (2) isotope chemical fractionation (Langer et al. 1984; Röllig & Ossenkopf 2013). The first operates in the far-ultraviolet (FUV)-illuminated, warm outer layers of molecular clouds (the so-called photodissociation regions, PDRs); the second operates in the cold, FUV-shielded inner regions of those molecular clouds. In past work, selective photodissociation of ^{13}CO with respect to ^{12}CO has been investigated as the cause of the high ^{12}CO/^{13}CO intensity ratios in (ultra)luminous infrared galaxies [(U)LIRGs], but found unlikely for large masses of their molecular gas reservoirs (Casoli et al. 1992).

This can be shown for the metal-rich, high-pressure molecular gas reservoirs expected in merger/starbursts such as local (U)LIRGs and distant submm-selected galaxies (SMGs). Indeed, in such metal-rich environments, it can be shown that the H_2 gas mass fraction expected to be in PDRs (the only gas that could be affected by selective photodissociation effects) is small, and thus cannot perturb global isotopologue abundance ratios away from the elemental

Table 1. $^{12}CO/^{13}CO$, $^{12}CO/C^{18}O$ and $^{13}CO/C^{18}O$ abundance ratios for external galaxies, compiled from the literature.

Name	Type	Redshift	SFR[a] ($M_\odot$ yr^{-1})	$^{12}CO/^{13}CO$	$^{12}CO/C^{18}O$	$^{13}CO/C^{18}O$	Method	References[b]
SPT stacking[c]	SMG	3.0	500–2000	100–200	>100–200	>1 (3σ)	LVG modelling	1
Cloverleaf	QSO	2.5579	1000	300–10 000	–	–	LVG modelling	2, 3
MA2.53	DLA	2.525	–	>40	–	–	Optical absorption	4
Eyelash[d]	SMG	2.3	400	100[e]	100	0.8	LVG modelling	5
MA1.15	DLA	1.15	–	>53 (3σ)	–	–	Optical absorption	6
MA0.89	Spiral	0.89	–	27 ± 2	52 ± 4	1.9	Absorption + LVG modelling	7
MA0.68	Spiral	0.68	–	38 ± 5	~80	~2	Absorption + LVG modelling	8
Mrk 231	ULIRG	0.042 170	100	100	100	1.0	CN modelling	9
NGC 6240	ULIRG	0.0245	100	300–500	–	1.6	LVG modelling	10, 11
Arp 193	ULIRG	0.023 299	100	~150	–	–	LVG modelling	10
VV 114	LIRG	0.020 067	48	229	–	–	LVG modelling	12
Arp 220	ULIRG	0.018 126	220	–	70–130	1.0	OH and H_2O absorption	13
Arp 220	ULIRG	0.018 126	220	–	>80–100	1.0	Line ratio limits	14
NGC 1614	LIRG	0.015 938	41	130	–	>6.6	LVG modelling	15
LMC	Dwarf	0.000 927	one clump	49	2000	27±9	LVG modelling	16, 17
NGC 253	LIRG	0.000 811	2.8	>56	145 ± 36	2.6	Line ratio limits + CN modelling	18, 9, 19
M82	LIRG	0.000 677	4.6	>138	>350	2.2-3.7	Line ratio limits + CN modelling	18, 20, 21
NGC 1068	LIRG	0.003 793	25	–	–	3.33		22
NGC 1614	LIRG	0.015 938	55	>36.5	>80	>2.2		23
NGC 4945	LIRG	0.001 878	<7.8	>17	>61	3.6		24
Cen A	Radio	0.001 825	0.16	17	>56	>3	Absorption + modelling	25, 26
NGC 2903	Normal	0.001 834	2.7	>10	–	>7 (3σ)		27
IC 860	LIRG	0.011 164	25	>20	>20	1		28
NGC 3079	Normal	0.003 723	9.3	>17	>91.5	5.4		28
NGC 4194	LIRG	0.008 342	20	>18.7	>47	>2.5		28
NGC 7469	LIRG	0.016 317	67	>21	>142	6.8		28
NGC 7771	LIRG	0.014 267	38	>14	>65	4.7		28
NGC 660	Normal	0.002 835	5.3	>17	>46	6.9		28
NGC 3556	Normal	0.002 332	4	>12.5	>161	12.9		28
NGC 7674	LIRG	0.028 924	54	>14.5	>40	2.8		28
UGC 2866	Radio	0.004 110	8	>21	>120	5.8		28
Circinus	Normal	0.001 448	8	>13	>54	5.1		29, 30, 31
IC 10	Normal	−0.001 161	0.2	>7	>100 (3σ)	>15		32, 33
IC 342	Normal	0.000 103	2.5	>10	>70	3-7		34
M51	Normal	0.002 000	4.5	>10	>46	4.5		35
Maffei 2	Normal	−0.000 057	0.26	>10	>43	4.3		36
NGC 1808	Normal	0.003 319	8.8	>17	>49	3		37
NGC 3256	LIRG	0.009 354	63	>33	>135	4		37
NGC 7552	LIRG	0.005 365	18	>14	>35	3		37
NGC 4826	Normal	0.001 361	0.2	>8	>21	4		37
NGC 2146	LIRG	0.002 979	20	>12.5	>36	3		37
NGC 4418	LIRG	0.007 268	20.7	–	–	8.3		38
IRAS 04296+2923 starburst	Normal	0.007 062	16	>21	>94	3.7		39
IRAS 04296+2923 CNZ	Normal	0.007 062	16	>16	>45	1.7		39
NGC 6946	Normal	0.000 133	2.5	>13.3	>21	2.5		40

Notes. [a]The star formation rates are from standard IMFs.

[b]1: Spilker et al. (2014); 2: Henkel et al. (2010); 3: Lutz et al. (2007); 4: Noterdaeme et al. (2017); 5: Danielson et al. (2013); 6: Levshakov et al. (2006); 7: Muller et al. (2006); 8: Wallström, Muller & Guélin (2016); 9: Henkel et al. (2014); 10: Papadopoulos et al. (2014); 11: Pasquali, Gallagher & de Grijs (2004); 12: Sliwa et al. (2013); 13: González-Alfonso et al. (2012); 14: Martín et al. (2011); 15: Sliwa et al. (2014); 16: Wang et al. (2009); 17: Heikkilä, Johansson & Olofsson (1998); 18: Martín et al. (2010); 19: Harrison, Henkel & Russell (1999); 20: Mao et al. (2000); 21: Tan et al. (2011); 22: Papadopoulos & Seaquist (1999); 23: König et al. (2016); 24: Curran et al. (2001); 25: Espada et al. (2010); 26: Salomé et al. (2016); 27: Muraoka et al. (2016); 28: Costagliola et al. (2011); 29: Zhang et al. (2014); 30: Davis (2014); 31: For, Koribalski & Jarrett (2012); 32: Nishimura et al. (2016); 33: Yin et al. (2010); 34: Meier & Turner (2001); 35: Watanabe et al. (2014); 36: Meier, Turner & Hurt (2008); 37: Aalto et al. (1995); 38: Costagliola et al. (2015); 39: Meier, Turner & Beck (2014); 40: Meier & Turner (2004).

[c]Stacking results of the strongly lensed SMGs found by the South Pole Telescope (SPT) survey. All galaxies have been shifted to $z = 3$. The $C^{18}O$ lines only have a 3σ upper limit, while the ^{13}CO lines were detected at the $\sim 3\sigma$ level. The infrared (IR) luminosity is $L_{IR} = 4.2 \times 10^{13}$ $L_\odot$, which translates to a star formation rate, SFR $\simeq 6000$ $M_\odot$ yr^{-1}. However, these are lensed systems; therefore, the inferred SFRs have been scaled down using a suitable magnification factor.

[d]We adopt the best-fitting results over the whole galaxy. The uncertainty is large (see fig. 7 of Danielson et al. 2013).

[e]Danielson et al. (2011) report a 3σ limit $^{12}CO/^{13}CO > 60$.

isotopic abundance ratios. Indeed, following the method developed in Papadopoulos et al. (2014, section 5.1, equation 6),

$$f_{\rm PDR} \sim 2 \times \left[1 - \left(1 - \frac{4A_{\rm v}^{\rm tr}}{3\langle A_{\rm v}\rangle}\right)^3\right], \quad (1)$$

where $A_{\rm v}^{\rm tr} = 1.086\,\xi_{\rm FUV}^{-1}\ln[1 + \Phi\, G_0^{\rm FUV}\, k_0/(n R_{\rm f})]$ is the visual extinction corresponding to a transition (between H I and H_2) column density, $\xi_{\rm FUV} = \sigma_{\rm FUV}/\sigma_{\rm V} \sim 2$–3 is the dust cross-section ratio for FUV and optical lights, $\Phi = 6.6 \times 10^{-6}\sqrt{\pi} Z^{1/2}\xi_{\rm FUV}$ is the H_2 self-shielding fraction over the H I/H_2 transition layer, $G_0^{\rm FUV}$ is the PDR radiation field, $k_0 = 4 \times 10^{-11}$ s^{-1} is the H_2 dissociation rate, n is the average gas density, $R_{\rm f} \sim 3 \times 10^{-17}$ cm^{-3} s^{-1} and $Z = 1$ (solar) is the metallicity.

We find the PDR gas mass fraction per cloud to be $f_{\rm PDR} \sim 0.004$–0.06 (H I+H_2) for the metal-rich and high-pressure (and thus high-density) molecular gas of (U)LIRGs. Even for less extreme conditions, with $n \sim 5 \times 10^3$ cm^{-3}, $T_{\rm kin} \sim 20$ K, $P_{\rm e}/k_{\rm B} \sim 10^5$ cm^{-3}, we obtain $f_{\rm PDR} \sim 0.11$–0.17, of which only around half will be molecular gas, and a smaller fraction still will be affected by selective photodissociation of the rarer isotopologues. These small gas mass fractions ensure that selective photodissociation cannot play a major role for the bulk of the molecular gas found in dust-enshrouded starbursts. Finally, the fact that cloud-volumetric heating processes such as cosmic rays (CRs) and/or X-rays rather than (cloud surface)-heating FUV photons of PDRs seem to be responsible for the average thermal state of molecular gas in LIRGs (e.g. Panuzzo et al. 2010; van der Werf et al. 2010; Papadopoulos et al. 2012; Indriolo et al. 2017) makes it even more unlikely that an FUV-driven isotopologue selective dissociation process affects much of their molecular gas mass reservoirs.

At the cold end, isotope fractionation operates via exothermic isotope-exchange chemical reactions whose $T_{\rm kin}$ sensitivity lies in a range where molecular gas is found in ordinary spirals. Indeed, the three most important reactions behind the theory of ^{12}C/^{13}C fractionation are

$$^{13}C^+ + CO \rightleftharpoons C^+ + {}^{13}CO + 35\,K, \quad (2)$$

$$^{13}CO + HCO^+ \rightleftharpoons CO + H^{13}CO^+ + 17\,K, \quad (3)$$

$$^{13}C^+ + CN \rightleftharpoons C^+ + {}^{13}CN + 31\,K \quad (4)$$

(Röllig & Ossenkopf 2013; Tunnard et al. 2015, and references therein). The effects of isotope fractionation have recently been invoked to explain the isotopologue ^{13}CO, ^{12}CO and H^{13}CN, H^{12}CN line ratios observed in the (U)LIRG, NGC 6240 (Tunnard et al. 2015). However, this work did not consider the minimum $T_{\rm kin}$ set by the CR heating that is expected to be ubiquitous in the environments of starbursts, and argued that dense ($n = 10^6$ cm^{-3}) and very cold ($T_{\rm kin} = 10$ K) gas comprises the most massive phase of H_2 in NGC 6240. At such low temperatures, isotopic fractionation can indeed operate (e.g. Röllig & Ossenkopf 2013), but these conditions can only be found in dense gas cores, deep inside giant molecular clouds in the relatively quiescent Milky Way, with its low levels of average CR energy density.

Using fig. 1 from Papadopoulos et al. (2011), we find that $T_{\rm kin} = 20$–30 K is the minimum value set by CRs in FUV-shielded dense gas in (U)LIRGs, where CR energy densities are 100–500 times that in the Galaxy and $n = 10^5$ cm^{-3}. This temperature can be higher still if turbulent gas heating and/or heating from IR-heated dust remains significant in such regions. Moreover, the discovery of high HCN($J = 4$–3) brightness temperatures in high-resolution ALMA maps of the (U)LIRG, Arp 220 (Project: 2015.1.00702S, PI: L. Barcos-Munoz), with $T_{\rm b}$ HCN ($J = 1$–0) ~ 70–80 K sets a lower limit for $T_{\rm kin}$ in the dense, line-emitting HCN gas that is well above the regime where isotope fractionation can operate.

For NGC 6240, ALMA observations (Project: 2012.00077.S, PI: N. Scoville) give $T_{\rm b}$ HCN ($J = 4$–3) ~ 3 K at 70 pc spatial resolution; thus, for its observed HCN(4–3/1–0) global brightness ratio of 0.18, it would be $T_{\rm b}$ HCN ($J = 1$–0) ~ 17 K as the corresponding lower limit for the temperature of the dense gas. This is well above the temperature range where chemical fractionation can operate. On the other hand, the $T_{\rm dust} \sim 40$ K found in NGC 6240 (Lisenfeld, Isaak & Hills 2000), and for a normal gas-to-dust mass ratio, there is no room for a significant mass of colder dust. Since $T_{\rm kin} \geq T_{\rm dust}$ in the bulk of the ISM (irrespective of whether the energetics are FUV and/or CR driven), a scenario involving large amounts of gas at low temperatures and high densities (where chemical fractionation can operate) is highly unlikely. We thus conclude that isotope chemical fractionation cannot operate for the bulk of the molecular gas in star-forming galaxies.

Thus, the road is now clear to use global isotopologue abundance ratios to obtain the corresponding average isotope abundance ratios in the ISM of galaxies. Nevertheless, serious uncertainties remain, associated with the radiative transfer modelling of molecular line emission. Indeed, careful radiative transfer modelling is needed to obtain the range of isotopologue abundance ratios, such as [^{12}CO/^{13}CO], from multi-J ^{12}CO and ^{13}CO emission line observations. Even when multiple lines are available, degeneracies still remain (e.g. Papadopoulos et al. 2014). Better angular resolution is also needed to resolve the local variation of the isotopologue line ratios, which can be resolved easily with ALMA now (e.g. Jiménez-Donaire et al. 2017). In the age of ALMA, with its extraordinary sensitivity, angular resolution and flexible, wide-band correlator, simultaneous isotopologue line observations will allow such degeneracies to be considerably reduced. Moreover, using multi-J *and* multi-species isotopologue line observations to determine a single isotope ratio (e.g. ^{12}CO, ^{13}CO and H^{12}CN, H^{13}CN lines to determine ^{12}C/^{13}C – Paglione, Jackson & Ishizuki 1997) will further reduce the model degeneracies.

3 CHEMICAL EVOLUTION MODELS

The chemical evolution model for the Milky Way used in this study was established in a series of papers (Chiappini, Matteucci & Gratton 1997; Romano et al. 2000, 2010; Chiappini, Matteucci & Romano 2001; Spitoni et al. 2015; see also Matteucci & Greggio 1986; Matteucci & François 1989) to which we refer the reader for a thorough discussion of the adopted formalism, the basic equations and the assumptions. It is a multi-zone model, where the Galactic disc is divided into several concentric annuli that evolve at different rates; this ensures the establishment of a Galactic abundance gradient.

For the other galaxies, we run simpler single-zone models. We do not aim to reproduce the CNO isotopic data available for each specific object; rather, we seek to give a broad overview of how the CNO isotopic ratios are expected to evolve in systems with different star formation histories and/or stellar IMFs. In these models, fresh gas is accreted according to an exponentially decreasing law, $d\mathscr{M}_{\rm inf}/dt \propto e^{-t/\tau}$ – where $\mathscr{M}_{\rm inf}$ is the total mass accreted and τ is the infall time-scale – and turned into stars following a Kennicutt–Schmidt relation, $\psi(t) = \nu\, \mathscr{M}_{\rm gas}(t)$, where ν is the star formation efficiency and $\mathscr{M}_{\rm gas}$ is the mass of neutral gas (Schmidt 1959; Kennicutt 1998). The free parameters, τ and ν, are set to

Table 2. Prescriptions for nucleosynthesis.

Model	LIMS	Super-AGB stars	Massive stars	Novae
1	Karakas (2010)	–	Nomoto et al. (2013)	No
2	Karakas (2010)	Doherty et al. (2014a,b)	Nomoto et al. (2013)	No
3	Karakas (2010)	–	Meynet & Maeder (2002b), Hirschi et al. (2005), Hirschi (2007), Ekström et al. (2008)	No
4	Karakas (2010)	Doherty et al. (2014a,b)	Meynet & Maeder (2002b), Hirschi et al. (2005), Hirschi (2007), Ekström et al. (2008)	No
5	Karakas (2010)	Doherty et al. (2014a,b)	Nomoto et al. (2013)	Yes

different values in order to frame different evolutionary paths. A more detailed description of the adopted formalism can be found in section 3.1 of Romano et al. (2015).

Specifically, we consider (i) a template for massive systems ($\mathscr{M}_{\rm DM} = 10^{13}$ M$_\odot$, $\mathscr{M}_\star \sim 2 \times 10^{11}$ M$_\odot$) that accrete gas rapidly ($\tau = 0.05$ Gyr) and experience powerful starbursts ($\nu \simeq 1$–2 Gyr^{-1}) at high redshift, followed by passive evolution thereafter;[1] (ii) a template for massive spirals ($\mathscr{M}_{\rm DM} \simeq 10^{12}$ M$_\odot$, $\mathscr{M}_\star \sim 5 \times 10^{10}$ M$_\odot$) that accrete gas slowly ($\tau = 13$ Gyr) and experience steady star formation ($\nu \simeq 0.05$–0.1 Gyr^{-1}) over a Hubble time; (iii) a model similar to the latter, but for galaxies of lower mass ($\mathscr{M}_{\rm DM} \simeq 10^{11}$ M$_\odot$, $\mathscr{M}_\star \sim 10^{10}$ M$_\odot$) where secular evolution is followed suddenly by an extremely efficient ($\nu \simeq 20$ Gyr^{-1}) burst of star formation. The star formation histories of these systems are shown in the top panels of Fig. 7, for different choices of the stellar IMF (see the next paragraph; see also discussion in Section 4.2).

The probability that a newly born star has an initial mass within a given mass range is given by the Kroupa (2002) IMF, with a slope $x = 1.7$ for high masses, normalized to unity in the 0.1–100 M$_\odot$ range. For the starbursts, we also investigate the effects of an IMF skewed towards high masses ($x = 0.95$ in the high-mass regime), similar to the one proposed by Ballero et al. (2007) for the Galactic bulge.

All our computations avoid the instantaneous recycling approximation by detailed accounting of the finite stellar lifetimes. This is a necessary prerequisite for a proper treatment of elements that are produced on different time-scales by stars of different initial masses and chemical compositions. The nucleosynthetic outcomes of binary stars exploding as Type Ia supernovae (SNe Ia) and novae are included in our computations, adopting the single-degenerate scenario for their progenitors (Matteucci & Recchi 2001, and references therein) for SNe Ia and our previous work (Romano et al. 1999, 2001; based on D'Antona & Matteucci 1991) for novae. Since CNO elements are produced in negligible amounts in SN Ia explosions (Iwamoto et al. 1999), the exact choice of the route leading to such events does not affect the results presented in this paper. Classical novae, instead, are thought to significantly overproduce ^{13}C, ^{15}N and ^{17}O with respect to their solar abundances (e.g. José & Hernanz 2007) making assumptions about their precursors a much more thorny problem (see the next section).

The adopted nucleosynthesis prescriptions are summarized in Table 2. The stellar yields for low- and intermediate-mass stars are from Karakas (2010). For massive stars, we adopt the grid of yields suggested by Nomoto, Kobayashi & Tominaga (2013, Models 1, 2 and 5). However, since the important effects of stellar rotation are not accounted for in this case, we also consider the grid of CNO yields from fast-rotating massive stars provided by the Geneva group (Meynet & Maeder 2002b; Hirschi, Meynet & Maeder 2005; Hirschi 2007; Ekström et al. 2008, Models 3 and 4). Detailed yields for super-AGB stars (Doherty et al. 2014a,b) – often neglected in chemical evolution studies – are implemented in Models 2, 4 and 5, while nova nucleosynthesis – also disregarded in most studies – is included in one case (Model 5). All the adopted yields for single stars are dependent on mass and metallicity. For novae, we assume average yields, independent of mass and metallicity (see discussion in Section 4.1). The different sets of yields were all tested against the Milky Way data, while only the set labelled '1' was used in the models for the other galaxies.

[1] These objects would appear as SMGs (e.g. Smail, Ivison & Blain 1997) at redshifts $z \simeq 2$–3 and as 'red and dead' massive ellipticals at $z = 0$ (see, e.g., Toft et al. 2014).

4 RESULTS

4.1 Milky Way galaxy

In this section, we present the results of our chemical evolution models for the Milky Way. These models differ in their adopted nucleosynthesis prescriptions (see Table 2). First, we discuss the predictions of Models 1, 2, 3 and 4, where the CNO elements come only from single stars. We then analyse the results of Model 5, which includes CNO production during nova outbursts.

Fig. 1 shows the evolution of the carbon isotope ratio in the solar neighbourhood (left-hand panel) and its current behaviour across the Milky Way disc (right-hand panel) predicted by Models 1 (green lines), 2 (light green lines), 3 (black lines) and 4 (grey lines). Models 1 and 3, which do not include the contribution to C synthesis from super-AGB stars, successfully reproduce the solar data (Ayres et al. 2013); adding the super-AGB star contribution, the solar ^{12}C/^{13}C ratio is slightly underestimated (Models 2 and 4). However, one must be aware that the Sun probably moved to its current position from a birthplace closer to the Galactic Centre (Wielen et al. 1996) and its chemical composition may not quite reflect that of the local ISM 4.5 Gyr ago. All the models predict current ^{12}C/^{13}C ratios in the solar neighbourhood that agree with the average local ISM value (Milam et al. 2005), within the errors. Furthermore, Models 3 and 4, assuming CNO yields from fast-rotating massive stars, can account for the range of carbon isotope ratios of 'unmixed' halo stars (i.e. giant stars in which the mixing with the deep layers affecting the original CNO abundances is not expected to have occurred; Spite et al. 2006). This result was already discussed by Chiappini et al. (2008), who stressed the important role played by fast rotators as ISM enrichers at low metallicities. When looking at the C isotope ratio as a function of the distance from the Galactic Centre, $R_{\rm GC}$, however, we find that Models 1 and 2 *without fast rotators* perform better. They predict an increasing trend of the ratio with increasing Galactocentric distance, as is indeed observed (Wilson & Rood 1994; Boogert et al. 2000; Savage et al. 2002; Milam et al. 2005), whilst Models 3 and 4 predict a decrease in the 8–12 kpc Galactocentric distance range, followed by a flattening at the outermost radii. In order to explain the ^{12}C/^{13}C ratios of both halo stars and molecular clouds, we conclude that fast-rotating massive stars must be common in the early Universe, but must become rarer

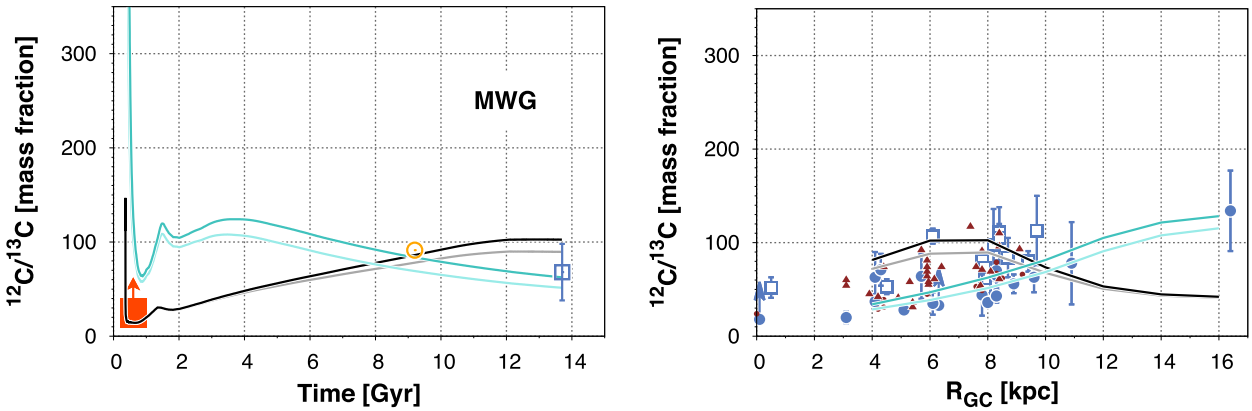

Figure 1. Left-hand panel: evolution of the carbon isotope ratio in the solar neighbourhood, predicted by Models 1 (green line), 2 (light green line), 3 (black line) and 4 (grey line). The red box encompasses the $^{12}C/^{13}C$ ratios of 'unmixed' halo stars (Spite et al. 2006). The solar (91.4 ± 1.3; Ayres et al. 2013) and local ISM values (68 ± 15; Milam et al. 2005) are denoted by different symbols and colours. Right-hand panel: radial behaviour of the $^{12}C/^{13}C$ ratio at the present time predicted by Models 1 (green line), 2 (light green line), 3 (black line) and 4 (grey line). $^{12}C/^{13}C$ ratios across the disc inferred from observations of CO, H_2CO (as taken from the compilation of Wilson & Rood 1994), CO_2 (Boogert et al. 2000) and CN (Savage et al. 2002; Milam et al. 2005) are shown as dots, filled triangles, open squares and filled circles, respectively.

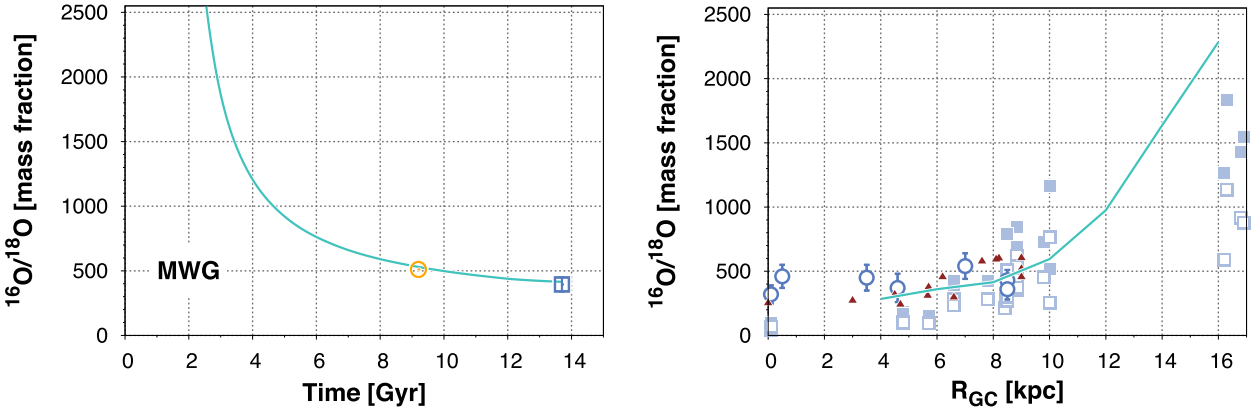

Figure 2. Left-hand panel: evolution of $^{16}O/^{18}O$ in the solar neighbourhood according to the predictions of Models 1 (green solid line) and 2 (light green line, hidden behind Model 1 predictions). Solar (511 ± 10; Ayres et al. 2013) and local ISM values (395 ± 56; Polehampton et al. 2005) are shown. Right-hand panel: current ratios of ^{16}O to ^{18}O against distance from the Galactic Centre predicted by Models 1 (green solid line) and 2 (light green line, hidden behind Model 1 predictions). Theoretical expectations are contrasted with formaldehyde data from the compilation of Wilson & Rood (1994, triangles), OH data from Polehampton et al. (2005, open circles) and CO data obtained by combining $^{13}C^{16}O/^{12}C^{18}O$ line ratios from Wouterloot et al. (2008) with the $^{12}C/^{13}C$ gradient suggested by Milam et al. (2005, filled squares: $J = 1$–0 transition; open squares: $J = 2$–1 transition).

when the metallicity exceeds [Fe/H] $\simeq -2$ dex. In our model, this metallicity threshold is reached only 40 Myr after the star formation begins, during the halo phase.

Models 1 and 2 also reproduce the $^{16}O/^{18}O$ ratios measured in the Sun (Ayres et al. 2013) and along the Galactic disc (Wilson & Rood 1994; Polehampton et al. 2005; Wouterloot et al. 2008, the latter in combination with the $^{12}C/^{13}C$ gradient of Milam et al. 2005) with the possible exception of the outermost regions (see Fig. 2, left- and right-hand panels, respectively). In the plots, Model 2 predictions are hidden behind those of Model 1 (which is expected since the two differ only in the treatment of super-AGB stars, while ^{16}O and ^{18}O are synthesized mostly in massive stars). The shortcomings of the models for $R_{GC} > 10$ kpc might be due to insufficient ^{18}O production from low-metallicity ([Fe/H] $\lesssim -1$ dex) stellar models. The $^{18}O/^{17}O$ ratios, on the other hand, are severely overestimated, even when considering the significant contribution to ^{17}O synthesis from super-AGB stars (Fig. 3). This may indicate the need for additional ^{17}O factories, which we naturally seek in nova systems. Novae are also thought to be powerful ^{15}N producers on a galactic scale.

In Model 5, we have added a contribution to the CNO synthesis from novae. The left-hand panels of Figs 4 and 5 show, respectively, the evolution of the $^{18}O/^{17}O$ and $^{14}N/^{15}N$ ratios in the solar neighbourhood; the radial behaviour of the same ratios at the present time is depicted in the right-hand panels. Model 5 predictions (orange solid lines) are compared to the relevant observations. The solar $^{18}O/^{17}O$ ratio (Ayres et al. 2013) can be explained by Model 5, which also fits the measurements across the disc (the lower-than-observed $^{18}O/^{17}O$ ratios predicted by the model for $R_{GC} > 12$ kpc likely arise from insufficient ^{18}O production from low-metallicity massive stars, rather than from oversynthesis of ^{17}O in nova outbursts – see the discussion in the previous paragraph). The model convincingly matches the nitrogen isotope ratios measured in solar wind ion samples by the *Genesis* spacecraft (Marty et al. 2011), in molecular clouds in the local ISM and across the whole Galactic disc (Adande & Ziurys 2012). The flattening of the theoretical $^{14}N/^{15}N$ gradient for $R_{GC} > 10$ kpc is due to the absence of a substantial primary ^{14}N component in the adopted yields for massive stars (Nomoto et al. 2013). While the need for significant primary ^{14}N

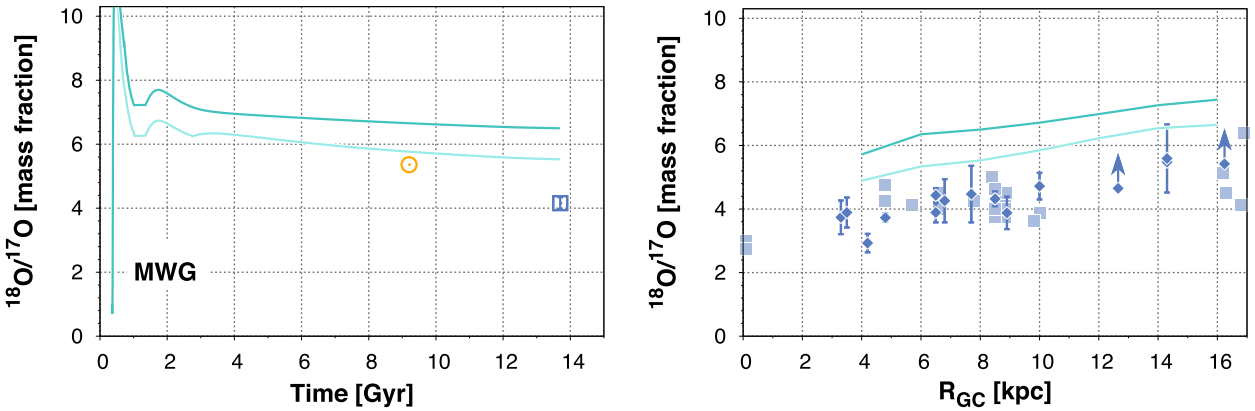

Figure 3. Left-hand panel: evolution of $^{18}O/^{17}O$ in the solar neighbourhood predicted by Models 1 (green line) and 2 (light green line) compared to the solar (5.36 ± 0.34, Sun symbol; Ayres et al. 2013) and local ISM values (4.16 ± 0.09, open square; Wouterloot et al. 2008). Right-hand panel: $^{18}O/^{17}O$ ratios across the disc at the present time. Theoretical predictions are shown together with ratios derived from CO lines by Wouterloot et al. (2008, filled squares) and Li et al. (2016, diamonds).

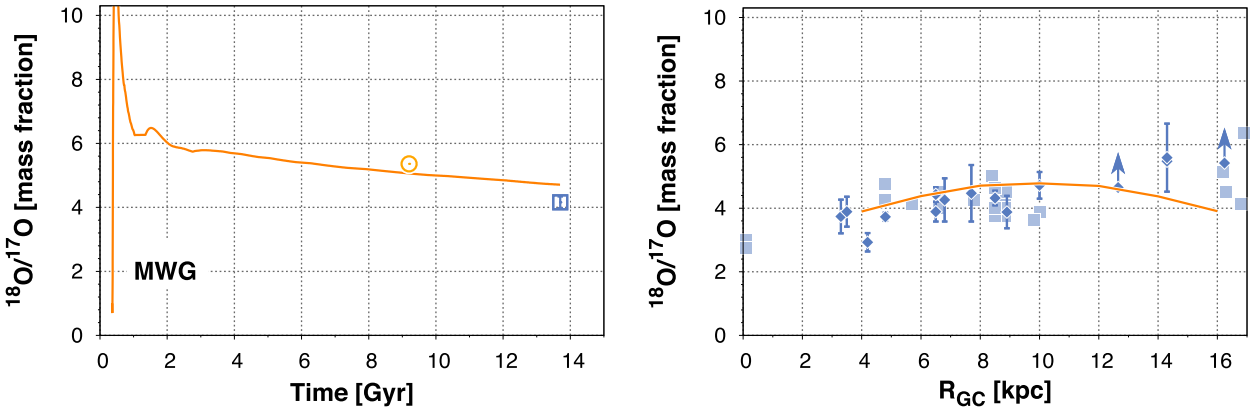

Figure 4. Same as Fig. 3, except that theoretical predictions (orange lines) are from Model 5 and include CNO production during thermonuclear runaways leading to nova eruptions.

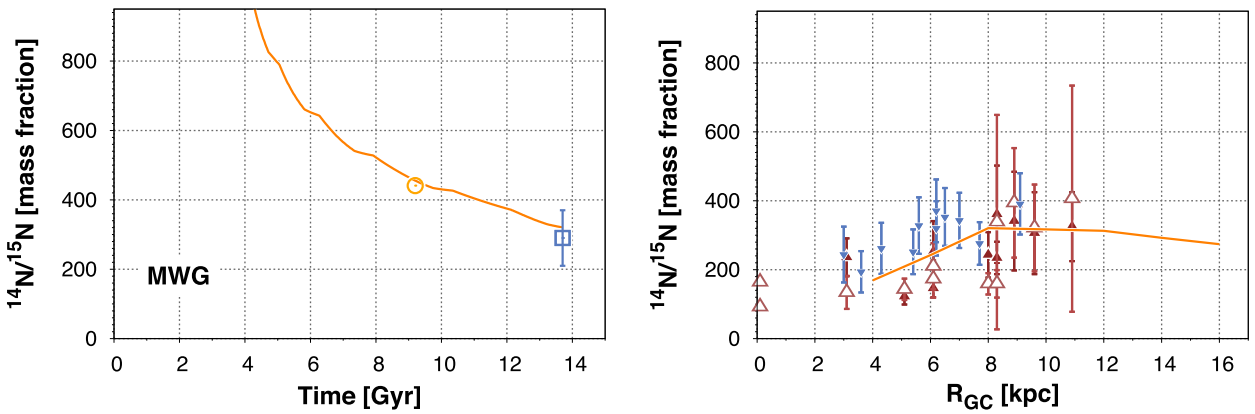

Figure 5. Left-hand panel: evolution of the nitrogen isotope ratio in the solar vicinity predicted by Model 5 (orange line). The Sun symbol and open square refer to the values of the ratio determined for the protosolar nebula (441±6; Marty et al. 2011) and local ISM (290±40; Adande & Ziurys 2012), respectively. Right-hand panel: nitrogen isotope ratios as a function of Galactocentric distance. The solid line is the present-day gradient from Model 5, while different symbols denote different observational estimates. Following Adande & Ziurys (2012, their table 4), filled triangles represent direct measurements using the hyperfine components of the CN isotopologues; open triangles indicate ratios obtained by combining $HN^{13}C/H^{15}NC$ data with $^{12}CN/^{13}CN$ measurements by Milam et al. (2005); upside-down triangles show ratios derived by applying the $^{12}CN/^{13}CN$ gradient suggested by Milam et al. (2005) to the HCN double isotopomer data of Dahmen et al. (1995).

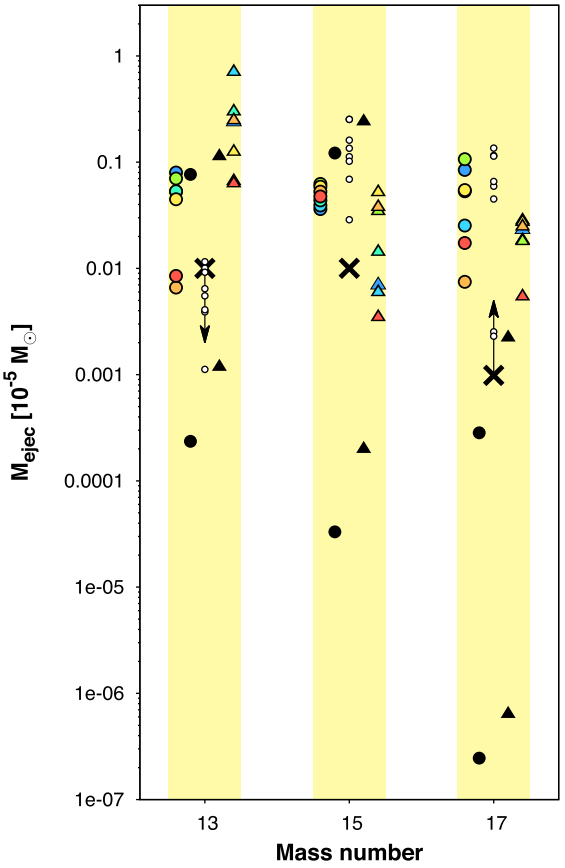

Figure 6. Average masses of ^{13}C, ^{15}N and ^{17}O ejected in a nova outburst (units of 10^{-5} $M_\odot$) required to explain the observed evolution of the CNO isotope ratios in the Milky Way in the context of our chemical evolution model ($\times$ signs) contrasted with elemental yields emerging from detailed hydrodynamic nova models for CO (triangles) and ONe (circles) white dwarfs (coloured symbols, José & Hernanz 1998; black symbols, Yaron et al. 2005; small open circles, Starrfield et al. 2009).

production from low-metallicity massive stars has been recognized for a long time (see e.g. Matteucci 1986, and references therein), more data are needed in order to assess the shape of the ^{14}N/^{15}N gradient at large Galactic radii, $R_{GC} > 12$ kpc, which would place important and independent constraints on the amount of primary nitrogen produced by massive stars in low-metallicity environments.

Only a few attempts have been made to include novae as additional CNO sources in Galactic chemical evolution models, even though allowing CNO production only from single stars fails to reproduce at least some of the CNO isotope abundance data available for the Milky Way (e.g. Romano & Matteucci 2003; Kobayashi et al. 2011). This reluctance is partly driven by the ill-constrained parameters that describe the evolution of the close, mass-transferring binary systems that lead to classical nova outbursts. Over the last 45 years, however, hydrodynamic simulations of nova outbursts by different groups – using different codes and reaction-rate libraries, and spanning different ranges of white dwarf masses and initial luminosities, mass-transfer rates from the main-sequence companions and mixing levels between the accreted envelope and the underlying white dwarf core – have generally found ejecta enriched in ^{13}C, ^{15}N and ^{17}O at a level that would significantly impact Galactic evolution (see José 2012, for a recent review). In Fig. 6, we show the masses ejected in the form of ^{13}C, ^{15}N and ^{17}O from nova models for CO (triangles) and ONe (circles) white dwarfs. Coloured symbols refer to models (José & Hernanz 1998) for different white dwarf masses and degrees of mixing between core and envelope, but fixed white dwarf luminosity and mass-accretion rate. The black symbols represent models for different masses and mass-transfer rates, but fixed white dwarf temperature from Yaron et al. (2005, their table 6). The small open circles refer to simulations of 1.25 $M_\odot$ white dwarfs and 1.35 $M_\odot$ white dwarfs using the same initial conditions but four different reaction-rate libraries for each mass (Starrfield et al. 2009). It is evident that the mass ejected in the form of a given element in one outburst may vary by several orders of magnitude, depending on the specific combination of parameters that produces the eruption.

Following Romano et al. (1999, and references therein), in Model 5 the birth rate of binary systems with the characteristics necessary to give rise to nova eruptions is computed as a fraction α of the white dwarf formation rate.[2] The value of α is fixed so as to have a current Galactic nova outburst rate of 20 yr^{-1}, consistent with the observed rate (20–34 yr^{-1}; Della Valle & Livio 1994). Computation of the theoretical nova outburst rate involves some knowledge of the average number of outbursts that a typical nova system is expected to experience; we take this number to be 10^4 (Bath & Shaviv 1978). The average masses ejected in the form of ^{13}C, ^{15}N and ^{17}O in a single eruption are fixed by the requirement of reproducing the observations of the CNO isotope ratios in the Milky Way. We find that the ejection of 10^{-7} $M_\odot$ of ^{15}N and 10^{-8} $M_\odot$ of ^{17}O in a single outburst leads to agreement between model and data. However, if current ^{18}O yields from massive stars are underestimated, the latter quantity should be regarded as a lower limit. In fact, in this case, novae should eject even higher amounts of ^{17}O to compensate for the increased ^{18}O production from massive stars. Now regarding ^{13}C, we can only set an upper limit of 10^{-7} $M_\odot$ per event, above which the predictions of Model 5 deviate significantly from measurements of ^{12}C/^{13}C ratios in the Galaxy. Our empirically determined nova yields are shown as $\times$ signs in Fig. 6.

4.2 Other galaxies

In this section, we deal with the interpretation of ^{12}C/^{13}C and ^{16}O/^{18}O ratios in other galaxies found using isotopologue line intensities available from the literature; we do not consider objects for which only lower limits are provided (see Section 2.2 and Table 1). In particular, we are interested in starburst galaxies, where the conditions of star formation differ from those typical in the local Universe (Papadopoulos 2010), and which may result in a top-heavy (flatter) IMF. As we will see, varying the IMF dramatically affects our predictions for CNO isotope evolution.

Already, 25 years ago, Faber, Worthey & Gonzales (1992) and Worthey, Faber & Gonzalez (1992) speculated that IMF variations could be responsible for the α-element overabundance inferred from measurements of Fe and Mg indices in their sample of elliptical galaxies: an IMF favouring more massive stars in more massive galaxies naturally leads to an overproduction of Mg (which is produced mostly by massive stars on short time-scales) with respect to Fe (produced mostly by SNe Ia with low-mass progenitors on longer time-scales) in larger systems, as observed (see also Matteucci & Tornambè 1987). However, they also stressed that differences in star formation time-scales and/or selective galactic winds could act in the same way, thereby leaving the issue of IMF variations unsettled

[2] This computation takes into account a delay time of 1 Gyr, to ensure that the white dwarfs have cooled enough to lead to strong nova outbursts.

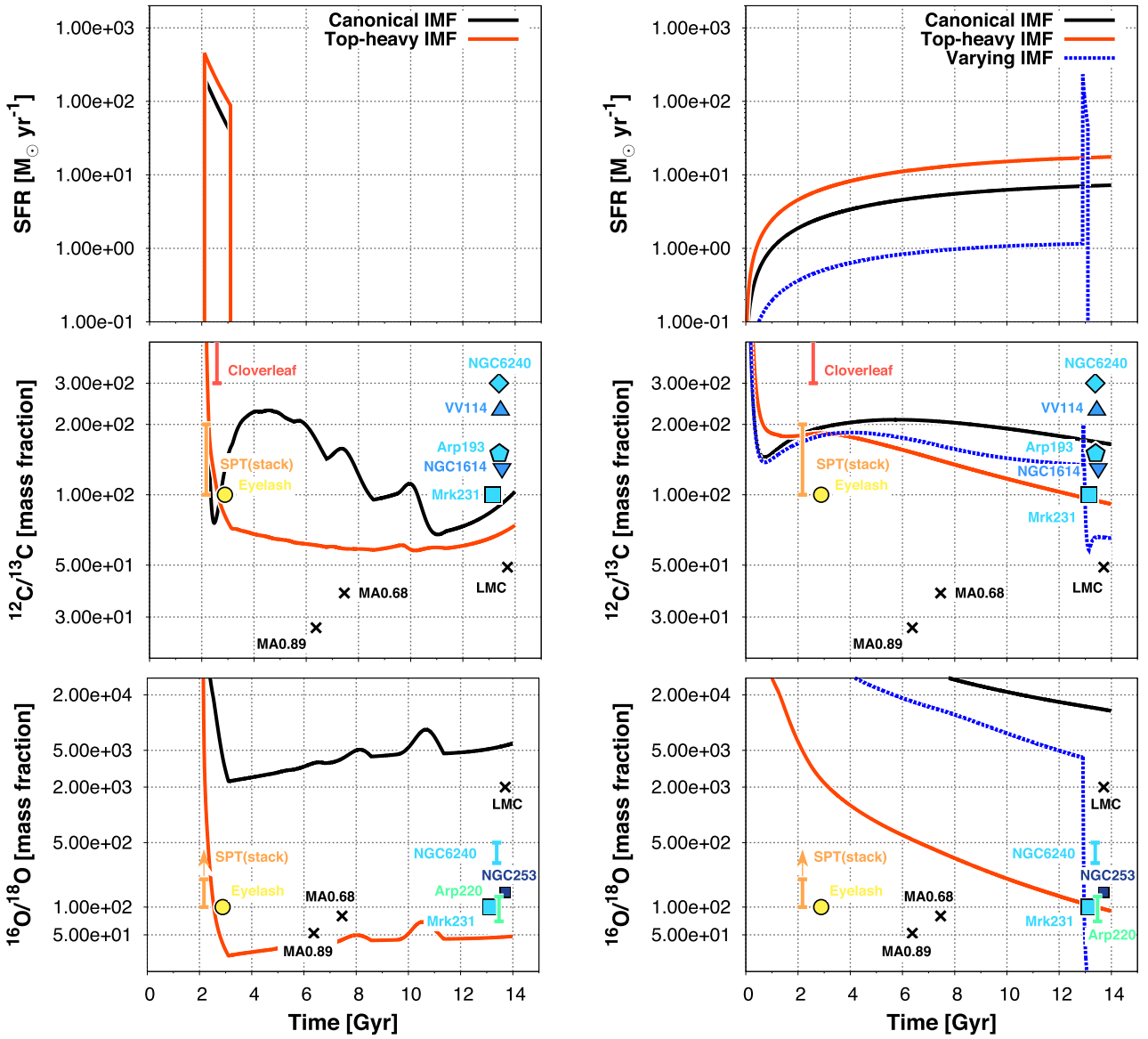

Figure 7. From top to bottom: star formation histories, evolution of the $^{12}C/^{13}C$ ratio and evolution of the $^{16}O/^{18}O$ ratio in the ISM of galaxies resembling either high-redshift SMGs (left-hand panels) or galaxies evolving quietly on a Hubble time (right-hand panels), apart from one object that experiences a late starburst (blue dashed lines). Different IMFs are considered, as labelled. The data (symbols and bars) are taken from Table 1 and colour-coded according to the level of star formation (see the text).

(see also Matteucci 1994). Nowadays, there is compelling observational evidence against the notion of a universal IMF (see e.g. the review in Weidner et al. 2013).

On the theoretical side, it has been suggested that when the SFR on a galactic scale exceeds 10 $M_\odot$ yr^{-1}, stars form in more massive and denser clusters, characterized by IMFs flatter than the canonical one; consequently, the galaxy-wide IMF also becomes top heavy (Weidner, Kroupa & Larsen 2004; Marks et al. 2012; Weidner et al. 2013). Such IMF variations lead to significant effects on many galaxy properties, ranging from the inferred stellar masses and SFRs (e.g. Clauwens, Schaye & Franx 2016) to the detailed chemical composition of the galaxy constituents (e.g. Recchi, Calura & Kroupa 2009).

Being the ratios of primary to secondary elements, the $^{12}C/^{13}C$ and $^{16}O/^{18}O$ isotope ratios are expected to show a pronounced dependence on the IMF slope.[3] In the middle and lower panels of Fig. 7, we show, respectively, the evolution of the $^{12}C/^{13}C$ and $^{16}O/^{18}O$ ratios predicted by our models, for different assumptions about the mass assembly and star formation history (see Section 3 and Fig. 7, upper panels), as well as the stellar IMF. The left-hand panels of Fig. 7 refer to template galaxies that suffer an intense burst of star formation at high redshift, then evolve passively thereafter, whereas the right-hand panels show the predictions for systems that experience secular evolution, followed by a late starburst in one case. In all panels, the black curves refer to models adopting a canonical IMF (Kroupa 2002, with $x = 1.7$ for the high masses), while the red ones are for models with a top-heavy IMF

[3] ^{13}C has both a primary and a secondary nucleosynthetic component.

(Ballero et al. 2007, with $x = 0.95$ in the high-mass regime). The blue dashed lines (right-hand panels only) refer to a template galaxy that forms stars according to a canonical IMF during most of its lifetime, with a sudden burst of star formation initiated later, inducing a top-heavy IMF during the burst. The nucleosynthesis prescriptions are the same as in Model 1 for the Galaxy, benchmarked by its good reproduction of the $^{12}C/^{13}C$ and $^{16}O/^{18}O$ data for the Milky Way. The data for the galaxies listed in Table 1 (detections only) are displayed as symbols and bars, and are colour-coded according to the intensity of the star formation on a rainbow scale where red and blue stand for higher and lower rates, respectively.

The models on the left ($\mathscr{M}_{\rm DM} = 10^{13}$ M$_\odot$) convert gas into stars at high redshift ($z \simeq 2$–3), in relatively brief ($\Delta t_{\rm burst} = 1$ Gyr) but extremely powerful starbursts (SFR $\simeq$ 100–450 M$_\odot$ yr^{-1}, for the top-heavy IMF; SFR $\simeq$ 40–200 M$_\odot$ yr^{-1}, for the canonical IMF). The differences in the SFR are dictated by the requirement that, when the star formation activity ceases, a stellar mass of $\mathscr{M}_\star \simeq 2 \times 10^{11}$ M$_\odot$ must be in place, independently of the choice of the IMF (see fig. 2 in Durkalec et al. 2015, for a relation between the stellar mass $\mathscr{M}_\star$ and the halo mass $\mathscr{M}_{\rm DM}$). The modelled galaxies are expected to show up as SMGs at high redshifts; indeed, the theoretical $^{12}C/^{13}C$ and $^{16}O/^{18}O$ ratios compare well with observational estimates of these ratios in high-redshift dusty, star-forming galaxies (Henkel et al. 2010; Danielson et al. 2013; Spilker et al. 2014).

In the starburst scenario, we see a large variation of the $^{12}C/^{13}C$ abundance ratio for the regular IMF, with this ratio remaining significantly higher than for the top-heavy IMF over a period of $\sim$ 3–10 Gyr. This is caused by the later release of large amounts of ^{13}C by intermediate-mass stars ($4 \leq M/M_\odot \leq 7$), and the much lower numbers of such stars in the case of a top-heavy IMF, where most of the ^{13}C injected into a galaxy's ISM occurs soon, from fast-evolving high-mass stars. This demonstrates the need for good chemical evolution models that avoid instantaneous element releases, and incorporate the stellar-physics-driven time-scales for the release of the various isotopes.

Nevertheless, the global $^{12}C/^{13}C$ abundance ratio does settle to very similar values for both types of IMF after a period of $\sim$11 Gyr. Here it is worth emphasizing that while the final anticipated global $^{12}C/^{13}C$ ratio seems rather insensitive to the underlying stellar IMF, values of $^{16}O/^{18}O$ as low as 100 found in the 'Cosmic Eyelash' (Swinbank et al. 2010; Danielson et al. 2013) and, possibly, in the stacked SMG spectrum in Spilker et al. (2014) are reached only by an IMF skewed towards massive stars (Fig. 7, lower-left panel). This conclusion is invariant of the assumed star formation history; in particular, we tested the case of a constant or increasing SFR with time, as well as a regime consisting of successive bursts separated by quiescent periods.

According to our computations, values of $^{12}C/^{13}C$ as high as 300 – or even higher measured towards the Cloverleaf quasar (Henkel et al. 2010) – indicate that the host galaxy is caught in a very early evolutionary phase, no later than $\sim$150 Myr from the beginning of the star formation episode; concordant with this dating, we predict that measurements of the globally averaged $^{16}O/^{18}O$ ratio in the Cloverleaf should yield values in excess of 2000.

In the right-hand panels of Fig. 7, we show the predictions of our models for smaller galaxies ($\mathscr{M}_{\rm DM} \simeq 10^{11}$–$10^{12}$ M$_\odot$, $\mathscr{M}_\star \simeq 1$–$5 \times 10^{10}$ M$_\odot$) that experience a quieter, continuous star formation; in the case of the model for the lowest mass, the evolution ends after a short ($\Delta t_{\rm burst} = 200$ Myr), vigorous starburst (SFR $\sim$ 100 M$_\odot$ yr^{-1}). As we already found for the high-redshift systems, it is immediately apparent that the $^{12}C/^{13}C$ and $^{16}O/^{18}O$ isotopic ratios for the low-redshift starbursts can be reproduced *simultaneously* only by assuming a top-heavy IMF. A canonical IMF leads to $^{16}O/^{18}O$ ratios that are higher than observed (Fig. 7, lower-right panel, black solid line). However, if the secular evolution – in which the stellar masses are distributed according to a canonical IMF – is followed by a burst of star formation with a flatter IMF, the $^{16}O/^{18}O$ ratio tends to values in agreement with those observed (Fig. 7, lower-right panel, blue dashed line). In the local Universe, such a sequence of galaxy evolution events could be mirrored by two gas-rich spirals evolving in isolation, before they merge inducing a strong merger/starburst late in their histories. This could indeed be the story behind local gas-rich starbursts, which makes the comparison of their global isotopologue ratios with the predictions of our 'starburst model' appropriate.

Finally, while a detailed analysis of the data available for local starbursts is beyond the scope of the present paper, it is worth noticing that our 'starburst model' predicts $^{12}C/^{13}C$ and $^{16}O/^{18}O$ ratios that span almost the full range of values covered by observations of local systems. Nevertheless, regardless of the details of the underlying star formation scenario, a top-heavy IMF seems necessary for building some part of their eventual stellar mass, with the low $^{16}O/^{18}O$ abundance ratios proving decisive. The fact that such ratios have been implied for many years, even for isolated (but vigorously star-forming) spiral galaxies (e.g. Papadopoulos et al. 1996), but nevertheless could not be attributed uniquely to a top-heavy IMF underscores the value of good CNO evolutionary models in setting such important constraints.

5 CONCLUSIONS

In this paper, we use state-of-the-art chemical evolution models to track the evolution of CNO isotopes in the ISM of galaxies. We take advantage of recently published stellar yields, as well as new isotopologue molecular line data for the Milky Way and many other galaxies. First, we use a multi-zone model for the Milky Way to re-assess the relative roles that AGB stars, massive stars and novae have in the production of the CNO elements, focusing on the rare isotopes. We find the following.

(i) In order to reproduce the $^{12}C/^{13}C$ ratios observed in both nearby halo stars and molecular clouds spanning a large range of Galactocentric distances, fast-rotating massive stars must be common in the early Universe, and become rarer when a metallicity threshold of [Fe/H] $\simeq -2$ dex is reached; this happens very early on in our model, about 40 Myr after the beginning of the star formation in the halo phase.

(ii) Super-AGB stars synthesize significant amounts of ^{17}O; yet, in order to bring the theoretical predictions for the $^{18}O/^{17}O$ ratio into agreement with the relevant Galactic data, one also needs to consider a contribution to ^{17}O synthesis from novae.

(iii) Novae are basic producers of ^{15}N; taking their contribution into account, we are able to reproduce both the declining trend of $^{14}N/^{15}N$ in the solar neighbourhood suggested by recent determinations of this ratio for the protosolar nebula (Marty et al. 2011) and the $^{14}N/^{15}N$ Galactic gradient recently revised by Adande & Ziurys (2012). Hydrogen ingestion into the helium shell of core-collapse supernovae has been suggested as an additional source of the rare ^{15}N isotope by Pignatari et al. (2015) who, however, do not provide a full grid of yields for use in chemical evolution models. This prevents us from testing their interesting proposal by means of our models.

(iv) By assuming yields from Karakas (2010) for low- and intermediate-mass stars, from Nomoto et al. (2013) for massive

stars, and average ejected masses of $M^{^{13}\mathrm{C}}_{\mathrm{ejec}} \leq 10^{-7}$ M$_\odot$, $M^{^{15}\mathrm{N}}_{\mathrm{ejec}} = 10^{-7}$ M$_\odot$ and $M^{^{17}\mathrm{O}}_{\mathrm{ejec}} \geq 10^{-8}$ M$_\odot$ per nova outburst, we find excellent agreement between most of our model predictions and the Milky Way CNO data; the model could be further constrained and improved when new data on the Galactic gradient at large radii become available.

Furthermore, we show that as far as galaxy-averaged abundance ratios are concerned, neither FUV-driven selective photodissociation nor chemical fractionation can seriously 'skew' isotopologue ratios away from isotopic ones. Then after selecting the best set of yields, we use single-zone models for other galaxies to investigate *qualitatively* the dependence of the ^{12}C/^{13}C and ^{16}O/^{18}O ratios on the star formation history and stellar IMF. By comparing the model predictions to observations of isotopologue (and thus isotopic) abundance ratios for the molecular gas reservoirs of high- and low-redshift starbursts, we conclude the following.

(i) In order to explain *simultaneously* the measurements of ^{12}C/^{13}C and ^{16}O/^{18}O ratios in starbursts, an IMF skewed towards high stellar masses is needed; this requirement is driven by the higher-than-observed ^{16}O/^{18}O ratios obtained with a canonical IMF, whilst the final ^{12}C/^{13}C ratio is not dramatically affected by the choice of the IMF.

(ii) The high ^{12}C/^{13}C ratios observed in some systems imply that either the galaxy is caught in its very early phases of evolution or, alternatively, that it is being 'rejuvenated' by a starburst that has erased the memory of the preceding evolution and reset the ^{12}C/^{13}C ratio to a high value; this, however, is possible only if the IMF becomes top heavy during the starburst.

(iii) For the host of the Cloverleaf quasar, at $z \simeq 2.5$, given the observational estimate of 300–10 000 for the ^{12}C/^{13}C ratio, we predict that a value of ^{16}O/^{18}O in excess of 2000 should be found.

(iv) Changing the details of the CNO isotope evolution or the assumptions about the histories of mass assembly and star formation does not affect the main conclusion that a top-heavy IMF is needed in starbursts.

In closing, we re-iterate how important these issues are for galaxy evolution, with ALMA now able to provide the data necessary to re-examine them, in the context of the concurrent CNO isotope evolution models, which can then give us the ages of starburst events and the prevailing stellar IMFs across cosmic time.

ACKNOWLEDGEMENTS

This research was supported by the Munich Institute for Astro- and Particle Physics (MIAPP) of the DFG cluster of excellence 'Origin and Structure of the Universe'. This work also benefited from the International Space Science Institute (ISSI) in Bern, thanks to the funding of the team 'The Formation and Evolution of the Galactic Halo' (PI: D. Romano). PPP is supported by an Ernest Rutherford Fellowship. RJI and ZYZ acknowledge support from ERC in the form of the Advanced Investigator Programme, 321302, COSMICISM.

REFERENCES

Aalto S., Booth R. S., Black J. H., Johansson L. E. B., 1995, A&A, 300, 369
Adande G. R., Ziurys L. M., 2012, ApJ, 744, 194
Akerman C. J., Carigi L., Nissen P. E., Pettini M., Asplund M., 2004, A&A, 414, 931
Audouze J., Lequeux J., Vigroux L., 1975, A&A, 43, 71
Ayres T. R., Lyons J. R., Ludwig H.-G., Caffau E., Wedemeyer-Böhm S., 2013, ApJ, 765, 46
Ballero S. K., Matteucci F., Origlia L., Rich R. M., 2007, A&A, 467, 123
Bath G. T., Shaviv G., 1978, MNRAS, 183, 515
Boesgaard A. M., 1968, ApJ, 154, 185
Boogert A. C. A. et al., 2000, A&A, 353, 349
Burbidge E. M., Burbidge G. R., Fowler W. A., Hoyle F., 1957, Rev. Mod. Phys., 29, 547
Casoli F., Dupraz C., Combes F., 1992, A&A, 264, 55
Cayrel R. et al., 2007, A&A, 473, L37
Charbonnel C., 1994, A&A, 282, 811
Charbonnel C., Zahn J.-P., 2007, A&A, 467, L15
Chiappini C., Matteucci F., Gratton R., 1997, ApJ, 477, 765
Chiappini C., Matteucci F., Romano D., 2001, ApJ, 554, 1044
Chiappini C., Hirschi R., Meynet G., Ekström S., Maeder A., Matteucci F., 2006, A&A, 449, L27
Chiappini C., Ekström S., Meynet G., Hirschi R., Maeder A., Charbonnel C., 2008, A&A, 479, L9
Clauwens B., Schaye J., Franx M., 2016, MNRAS, 462, 2832
Clayton D. D., Nittler L. R., 2004, ARA&A, 42, 39
Costagliola F. et al., 2011, A&A, 528, A30
Costagliola F. et al., 2015, A&A, 582, A91
Curran S. J., Johansson L. E. B., Bergman P., Heikkilä A., Aalto S., 2001, A&A, 367, 457
Cyburt R. H., Fields B. D., Olive K. A., Yeh T.-H., 2016, Rev. Mod. Phys., 88, 015004
D'Antona F., Matteucci F., 1991, A&A, 248, 62
Dahmen G., Wilson T. L., Matteucci F., 1995, A&A, 295, 194
Danielson A. L. R. et al., 2011, MNRAS, 410, 1687
Danielson A. L. R. et al., 2013, MNRAS, 436, 2793
Davis T. A., 2014, MNRAS, 445, 2378
Dearborn D., Tinsley B. M., Schramm D. N., 1978, ApJ, 223, 557
Della Valle M., Livio M., 1994, A&A, 286, 786
Doherty C. L., Gil-Pons P., Lau H. H. B., Lattanzio J. C., Siess L., 2014a, MNRAS, 437, 195
Doherty C. L., Gil-Pons P., Lau H. H. B., Lattanzio J. C., Siess L., Campbell S. W., 2014b, MNRAS, 441, 582
Durkalec A. et al., 2015, A&A, 576, L7
Edmunds M. G., Pagel B. E. J., 1978, MNRAS, 185, 77
Ekström S., Meynet G., Chiappini C., Hirschi R., Maeder A., 2008, A&A, 489, 685
Elbaz D. et al., 2011, A&A, 533, A119
Encrenaz P. J., Stark A. A., Combes F., Wilson R. W., 1979, A&A, 78, L1
Espada D. et al., 2010, ApJ, 720, 666
Faber S. M., Worthey G., Gonzales J. J., 1992, in Barbuy B., Renzini A., eds, Proc. IAU Symp. 149, The Stellar Populations of Galaxies. Kluwer, Dordrecht, p. 255
Fenner Y., Gibson B. K., Lee H.-C., Karakas A. I., Lattanzio J. C., Chieffi A., Limongi M., Yong D., 2003, PASA, 20, 340
For B.-Q., Koribalski B. S., Jarrett T. H., 2012, MNRAS, 425, 1934
Freeman K., Bland-Hawthorn J., 2002, ARA&A, 40, 487
Füri E., Marty B., 2015, Nat. Geosci., 8, 515
Gallagher A. J., Ludwig H.-G., Ryan S. G., Aoki W., 2015, A&A, 579, A94
García Pérez A. E., Aoki W., Inoue S., Ryan S. G., Suzuki T. K., Chiba M., 2009, A&A, 504, 213
Goldreich P., Kwan J., 1974, ApJ, 189, 441
González-Alfonso E. et al., 2012, A&A, 541, A4
Gratton R. G., Sneden C., Carretta E., Bragaglia A., 2000, A&A, 354, 169
Greve T. R., Papadopoulos P. P., Gao Y., Radford S. J. E., 2009, ApJ, 692, 1432
Harrison A., Henkel C., Russell A., 1999, MNRAS, 303, 157
Heikkilä A., Johansson L. E. B., Olofsson H., 1998, A&A, 332, 493
Henkel C., Mauersberger R., 1993, A&A, 274, 730
Henkel C., Mauersberger R., Wiklind T., Huettemeister S., Lemme C., Millar T. J., 1993, A&A, 268, L17
Henkel C., Downes D., Weiß A., Riechers D., Walter F., 2010, A&A, 516, A111
Henkel C. et al., 2014, A&A, 565, A3

Hirschi R., 2007, A&A, 461, 571
Hirschi R., Meynet G., Maeder A., 2005, A&A, 433, 1013
Hughes G. L., Gibson B. K., Carigi L., Sánchez-Blázquez P., Chavez J. M., Lambert D. L., 2008, MNRAS, 390, 1710
Iben I., Jr, 1975, ApJ, 196, 525
Ikarashi S. et al., 2015, ApJ, 810, 133
Indriolo N., Bergin E. A., Goicoechea J. R., Cernicharo J., Gerin M., Gusdorf A., Lis D. C., Schilke P., 2017, ApJ, 836, 117
Ivezić Ž., Beers T. C., Jurić M., 2012, ARA&A, 50, 251
Iwamoto K., Brachwitz F., Nomoto K., Kishimoto N., Umeda H., Hix W. R., Thielemann F.-K., 1999, ApJS, 125, 439
Jiménez-Donaire M. J. et al., 2017, ApJ, 836, L29
José J., 2012, Bull. Astron. Soc. India, 40, 443
José J., Hernanz M., 1998, ApJ, 494, 680
José J., Hernanz M., 2007, J. Phys. G: Nucl. Part. Phys., 34, R431
Karakas A. I., 2010, MNRAS, 403, 1413
Kennicutt R. C., Jr, 1998, ApJ, 498, 541
Kobayashi C., Karakas A. I., Umeda H., 2011, MNRAS, 414, 3231
König S., Aalto S., Muller S., Gallagher J. S., Beswick R. J., Xu C. K., Evans A., 2016, A&A, 594, A70
Kroupa P., 2002, in Grebel E. K., Brandner W., eds, ASP Conf. Ser. Vol. 285, Modes of Star Formation and the Origin of Field Populations. Astron. Soc. Pac., San Francisco, p. 86
Langer W. D., Penzias A. A., 1993, ApJ, 408, 539
Langer W. D., Graedel T. E., Frerking M. A., Armentrout P. B., 1984, ApJ, 277, 581
Levshakov S. A., Centurión M., Molaro P., Kostina M. V., 2006, A&A, 447, L21
Li H.-K., Zhang J.-S., Liu Z.-W., Lu D.-R., Wang M., Wang J., 2016, Res. Astron. Astrophys., 16, 47
Lind K., Meléndez J., Asplund M., Collet R., Magic Z., 2013, A&A, 554, A96
Lisenfeld U., Isaak K. G., Hills R., 2000, MNRAS, 312, 433
Lucas R., Liszt H., 1996, A&A, 307, 237
Lucas R., Liszt H., 1998, A&A, 337, 246
Lutz D. et al., 2007, ApJ, 661, L25
Mao R. Q., Henkel C., Schulz A., Zielinsky M., Mauersberger R., Störzer H., Wilson T. L., Gensheimer P., 2000, A&A, 358, 433
Marks M., Kroupa P., Dabringhausen J., Pawlowski M. S., 2012, MNRAS, 422, 2246
Martín S., Aladro R., Martín-Pintado J., Mauersberger R., 2010, A&A, 522, A62
Martín S. et al., 2011, A&A, 527, A36
Marty B., Chaussidon M., Wiens R. C., Jurewicz A. J. G., Burnett D. S., 2011, Science, 332, 1533
Matteucci F., 1986, MNRAS, 221, 911
Matteucci F., 1994, A&A, 288, 57
Matteucci F., D'Antona F., 1991, A&A, 247, L37
Matteucci F., François P., 1989, MNRAS, 239, 885
Matteucci F., Greggio L., 1986, A&A, 154, 279
Matteucci F., Recchi S., 2001, ApJ, 558, 351
Matteucci F., Tornambè A., 1987, A&A, 185, 51
Meier D. S., Turner J. L., 2001, ApJ, 551, 687
Meier D. S., Turner J. L., 2004, AJ, 127, 2069
Meier D. S., Turner J. L., Hurt R. L., 2008, ApJ, 675, 281
Meier D. S., Turner J. L., Beck S. C., 2014, ApJ, 795, 107
Meynet G., Maeder A., 2002a, A&A, 381, L25
Meynet G., Maeder A., 2002b, A&A, 390, 561
Milam S. N., Savage C., Brewster M. A., Ziurys L. M., Wyckoff S., 2005, ApJ, 634, 1126
Muller S., Guélin M., Dumke M., Lucas R., Combes F., 2006, A&A, 458, 417
Muller S. et al., 2014, A&A, 566, A112
Muraoka K. et al., 2016, PASJ, 68, 89
Nishimura Y., Shimonishi T., Watanabe Y., Sakai N., Aikawa Y., Kawamura A., Yamamoto S., 2016, ApJ, 829, 94
Nomoto K., Kobayashi C., Tominaga N., 2013, ARA&A, 51, 457
Noterdaeme P. et al., 2017, A&A, 597, A82
Osterbrock D. E., 1989, Astrophysics of Gaseous Nebulae and Active Galactic Nuclei. University Science Books, Mill Valley, CA
Paglione T. A. D., Jackson J. M., Ishizuki S., 1997, ApJ, 484, 656
Paglione T. A. D. et al., 2001, ApJS, 135, 183
Palmerini S., Busso M., Maiorca E., Guandalini R., 2009, PASA, 26, 161
Panuzzo P. et al., 2010, A&A, 518, L37
Papadopoulos P. P., 2010, ApJ, 720, 226
Papadopoulos P. P., Seaquist E. R., 1998, ApJ, 492, 521
Papadopoulos P. P., Seaquist E. R., 1999, ApJ, 516, 114
Papadopoulos P. P., Seaquist E. R., Scoville N. Z., 1996, ApJ, 465, 173
Papadopoulos P. P., Thi W.-F., Miniati F., Viti S., 2011, MNRAS, 414, 1705
Papadopoulos P. P., van der Werf P. P., Xilouris E. M., Isaak K. G., Gao Y., Mühle S., 2012, MNRAS, 426, 2601
Papadopoulos P. P. et al., 2014, ApJ, 788, 153
Pasquali A., Gallagher J. S., de Grijs R., 2004, A&A, 415, 103
Penzias A. A., Jefferts K. B., Wilson R. W., 1971, ApJ, 165, 229
Pignatari M. et al., 2015, ApJ, 808, L43
Placco V. M., Frebel A., Beers T. C., Stancliffe R. J., 2014, ApJ, 797, 21
Polehampton E. T., Baluteau J.-P., Swinyard B. M., 2005, A&A, 437, 957
Prantzos N., Aubert O., Audouze J., 1996, A&A, 309, 760
Recchi S., Calura F., Kroupa P., 2009, A&A, 499, 711
Rickard L. J., Blitz L., 1985, ApJ, 292, L57
Ritchey A. M., Federman S. R., Lambert D. L., 2015, ApJ, 804, L3
Roederer I. U., Lawler J. E., Sneden C., Cowan J. J., Sobeck J. S., Pilachowski C. A., 2008, ApJ, 675, 723
Röllig M., Ossenkopf V., 2013, A&A, 550, A56
Romano D., Matteucci F., 2003, MNRAS, 342, 185
Romano D., Matteucci F., Molaro P., Bonifacio P., 1999, A&A, 352, 117
Romano D., Matteucci F., Salucci P., Chiappini C., 2000, ApJ, 539, 235
Romano D., Matteucci F., Ventura P., D'Antona F., 2001, A&A, 374, 646
Romano D., Karakas A. I., Tosi M., Matteucci F., 2010, A&A, 522, A32
Romano D., Bellazzini M., Starkenburg E., Leaman R., 2015, MNRAS, 446, 4220
Sage L. J., Isbell D. W., 1991, A&A, 247, 320
Sage L. J., Mauersberger R., Henkel C., 1991, A&A, 249, 31
Salomé Q., Salomé P., Combes F., Hamer S., Heywood I., 2016, A&A, 586, A45
Savage C., Apponi A. J., Ziurys L. M., Wyckoff S., 2002, ApJ, 578, 211
Schmidt M., 1959, ApJ, 129, 243
Scoville N. Z., Solomon P. M., 1974, ApJ, 187, L67
Shirley Y. L., 2015, PASP, 127, 299
Simpson J. M. et al., 2017, ApJ, 839, 58
Sliwa K. et al., 2013, ApJ, 777, 126
Sliwa K., Wilson C. D., Iono D., Peck A., Matsushita S., 2014, ApJ, 796, L15
Smail I., Ivison R. J., Blain A. W., 1997, ApJ, 490, L5
Smiljanic R., Gauderon R., North P., Barbuy B., Charbonnel C., Mowlavi N., 2009, A&A, 502, 267
Spilker J. S. et al., 2014, ApJ, 785, 149
Spite M., Spite F., 2010, in Charbonnel C., Tosi M., Primas F., Chiappini C., eds, Proc. IAU Symp. 268, Light Elements in the Universe. Cambridge Univ. Press, Cambridge, p. 201
Spite M. et al., 2006, A&A, 455, 291
Spitoni E., Romano D., Matteucci F., Ciotti L., 2015, ApJ, 802, 129
Starrfield S., Iliadis C., Hix W. R., Timmes F. X., Sparks W. M., 2009, ApJ, 692, 1532
Swinbank A. M. et al., 2010, Nature, 464, 733
Tan Q.-H., Gao Y., Zhang Z.-Y., Xia X.-Y., 2011, Res. Astron. Astrophys., 11, 787
Timmes F. X., Woosley S. E., Weaver T. A., 1995, ApJS, 98, 617
Toft S. et al., 2014, ApJ, 782, 68
Tosi M., 1982, ApJ, 254, 699
Tunnard R., Greve T. R., Garcia-Burillo S., Graciá Carpio J., Fuente A., Tacconi L., Neri R., Usero A., 2015, ApJ, 815, 114
van der Werf P. P. et al., 2010, A&A, 518, L42
Wall W. F., Jaffe D. T., Bash F. N., Israel F. P., Maloney P. R., Baas F., 1993, ApJ, 414, 98
Wallström S. H. J., Muller S., Guélin M., 2016, A&A, 595, A96

Wang M., Chin Y.-N., Henkel C., Whiteoak J. B., Cunningham M., 2009, ApJ, 690, 580
Wasserburg G. J., Boothroyd A. I., Sackmann I.-J., 1995, ApJ, 447, L37
Watanabe Y., Sakai N., Sorai K., Yamamoto S., 2014, ApJ, 788, 4
Weidner C., Kroupa P., Larsen S. S., 2004, MNRAS, 350, 1503
Weidner C., Kroupa P., Pflamm-Altenburg J., Vazdekis A., 2013, MNRAS, 436, 3309
Wielen R., Fuchs B., Dettbarn C., 1996, A&A, 314, 438
Wiklind T., Combes F., 1995, A&A, 299, 382
Wiklind T., Combes F., 1996, A&A, 315, 86
Wilson T. L., Matteucci F., 1992, A&AR, 4, 1
Wilson T. L., Rood R., 1994, ARA&A, 32, 191
Worthey G., Faber S. M., Gonzalez J. J., 1992, ApJ, 398, 69
Wouterloot J. G. A., Henkel C., Brand J., Davis G. R., 2008, A&A, 487, 237
Yaron O., Prialnik D., Shara M. M., Kovetz A., 2005, ApJ, 623, 398
Yin J., Magrini L., Matteucci F., Lanfranchi G. A., Gonçalves D. R., Costa R. D. D., 2010, A&A, 520, A55
Young J. S., Sanders D. B., 1986, ApJ, 302, 680
Young E. D., Gounelle M., Smith R. L., Morris M. R., Pontoppidan K. M., 2011, ApJ, 729, 43
Zhang Z.-Y. et al., 2014, A&A, 568, A122
Zinner E., 2014, in Davis A. M., ed., Treatise on Geochemistry, 2nd edn. Vol. 1, Meteorites and Cosmochemical Processes. Elsevier, Oxford, p. 181

This paper has been typeset from a TEX/LATEX file prepared by the author.